Optimal vortex formation as an index of cardiac health

Morteza Gharib[†‡], Edmond Rambod[†], Arash Kheradvar[†], David J. Sahn[§], and John O. Dabiri[†]

[†]Graduate Aeronautical Laboratories and Bioengineering, California Institute of Technology, Pasadena, CA 91125; and [§]Pediatric Cardiology, Oregon Health Science University, Portland, OR 97239

Communicated by Anatol Roshko, California Institute of Technology, Pasadena, CA, January 27, 2006 (received for review August 24, 2005)

Heart disease remains a leading cause of death worldwide. Previous research has indicated that the dynamics of the cardiac left ventricle (LV) during diastolic filling may play a critical role in dictating overall cardiac health. Hence, numerous studies have aimed to predict and evaluate global cardiac health based on quantitative parameters describing LV function. However, the inherent complexity of LV diastole, in its electrical, muscular, and hemodynamic processes, has prevented the development of tools to accurately predict and diagnose heart failure at early stages, when corrective measures are most effective. In this work, it is demonstrated that major aspects of cardiac function are reflected uniquely and sensitively in the optimization of vortex formation in the blood flow during early diastole, as measured by a dimensionless numerical index. This index of optimal vortex formation correlates well with existing measures of cardiac health such as the LV ejection fraction. However, unlike existing measures, this previously undescribed index does not require patient-specific information to determine numerical index values corresponding to normal function. A study of normal and pathological cardiac health in human subjects demonstrates the ability of this global index to distinguish disease states by a straightforward analysis of noninvasive LV measurements.

cardiac dysfunction | left ventricle | mitral flow | biofluid dynamics

Previous research has indicated that dynamics of the cardiac left ventricle (LV) during diastolic filling play a critical role in dictating overall cardiac health (1–8). The flow of blood from the atrium to the ventricle of the left heart during early diastolic filling, known as the E wave, has been observed in both *in vivo* and *in vitro* studies to cause the formation of a rotating fluid mass called a vortex ring (9–11, Fig. 1 *a* and *b*). This process of vortex ring formation has been studied extensively in *in vitro* experiments (12–15), where it has been demonstrated that fluid transport by vortex ring formation is more efficient than by a steady, straight jet of fluid (16). Furthermore, it was recently discovered that energetic constraints limit the maximum growth of individual vortex rings (14).

These results suggest the possibility that vortex ring formation may be optimized in naturally occurring fluid transport processes, especially in biological systems that depend on efficient fluid transport for their survival. In ref. 17, *in vivo* and *in vitro* data were used to support the notion that, in principle, the vortex formation process can dictate optimal kinematics of any biological fluid transport system, including the human heart.

In this work, we test the hypothesis that the process of vortex ring formation during early LV diastole affects cardiac health and also serves as an indicator of cardiac health. To quantify the process of vortex ring formation and its potential optimization, a quantitative index is required. The index is most useful if it is dimensionless, so that it can be compared across patient groups. Existing dimensionless measures of cardiac health, such as the ratio index of diastolic blood flow (i.e., the relative magnitude of blood flow during the E wave and the subsequent atrial contraction A wave), cannot be interpreted without considering patient-specific effects, e.g., the pseudonormalization process that occurs in the transition from mild to moderate dysfunction (18).

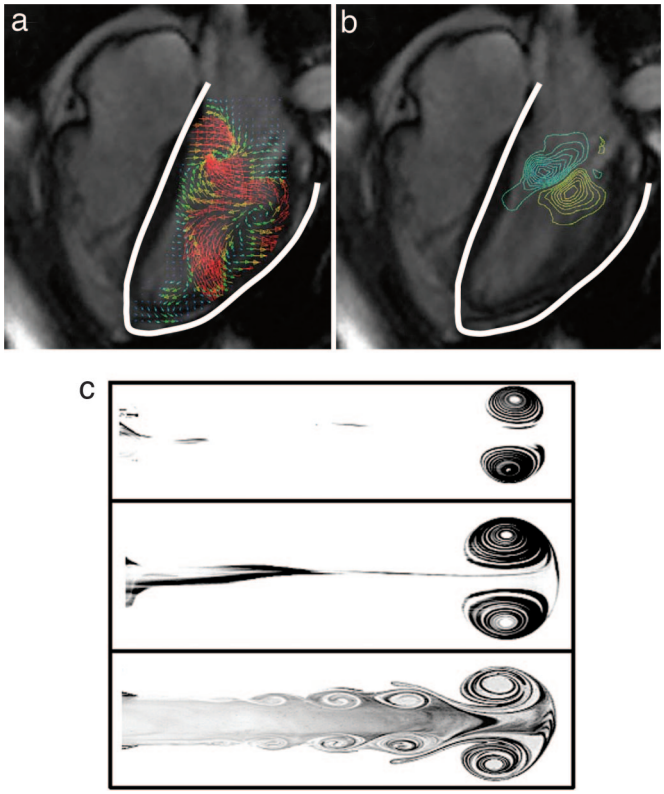

Fig. 1. Vortex ring formation *in vivo* and *in vitro*. (*a* and *b*) Map of *in vivo* blood flow velocity vectors and vorticity (rotation and shear) contours in the LV of a human heart during diastole. Images were obtained by magnetic resonance imaging of a healthy adult (courtesy of the Vascular Imaging Research Center, Department of Radiology, Veterans Affairs Medical Center/University of California, San Francisco). For emphasis, the LV boundary is indicated by a white line. Vortical patterns are indicated by the orientation of velocity vectors and by vorticity contours. Blue and yellow contours indicate clockwise and counterclockwise fluid rotation, respectively. (*c*) Fluorescent dye images of *in vitro* vortex ring formation in fluid jets with increasing vortex formation time. (*Top*) $T = 2.0$. (*Middle*) $T = 3.8$. (*Bottom*) $T = 14.5$. For $T > 4$, vortex ring growth terminates and fluid is subsequently ejected in a trailing jet. Figure is adapted from ref. 14.

Results and Discussion

A dimensionless numerical index has been previously defined to characterize vortex rings formed by fluid ejected from a rigid tube (14). This vortex formation time, $T = \overline{U(t)} \cdot t/D = L/D$, is

Conflict of interest statement: No conflicts declared.

Abbreviations: DCM, dilated cardiomyopathy; LV, left ventricle.

[‡]To whom correspondence should be addressed. E-mail: mgharib@caltech.edu.

determined based on the time-averaged speed of the fluid flow [$\overline{U(t)}$], the duration of fluid ejection (t), and the diameter of the orifice through which the fluid is ejected (D). In effect, the vortex formation time is a measure of the length-to-diameter ratio (L/D) of the ejected fluid column. A vortex ring will continue to grow larger during the process of fluid transport until a vortex formation time $T \approx 4$ is reached (Fig. 1*c*). After this point, the vortex ring is unable to grow larger because of energetic constraints (14, 19, 20), and ejected fluid subsequently forms a trailing jet behind the vortex ring. The transport of fluid by the trailing jet is less efficient than fluid transport by the vortex ring (16). Therefore, vortices are optimized for efficient fluid transport when formed during a vortex formation time $T \approx 4$, i.e., the largest possible vortex without formation of a trailing jet.

In the left heart, blood flow from the atrium to the ventricle passes the mitral valve leaflets, which form a time-varying exit diameter $D(t)$ as opposed to the constant diameter studied in the experiments noted above and in numerical simulations. The effect of a time-varying exit diameter on the vortex formation process was recently studied *in vitro* (21), where it was shown that for temporal increases in exit diameter (e.g., the opening of the mitral valve), the vortex formation time corresponding to maximum vortex growth remains unchanged at $T \approx 4$. However, to reach this conclusion, the definition of the dimensionless numerical index must be revised to incorporate the time history of the exit diameter: $T^* = \overline{U(t)/D(t)}\cdot t$, where the time average is now computed for the ratio of the instantaneous flow speed and exit diameter (17, 21). With this amendment, patterns of exit diameter variation as a function of vortex formation time $D(T^*)$ have been devised (17), which use optimal vortex formation to maximize either the efficiency of fluid transport or the total momentum (impulse) delivered to the flow by a biological pump. In ref. 17, the optimization of vortex formation during squid swimming was deduced, and a similar effect during cardiac function was hypothesized because similar vortex ring structures exist in both cases.

As mentioned previously, we hypothesize that disease-related dysfunctions in steps that precede complete LV diastolic failure are reflected in the dynamics of transmitral blood flow during early LV diastole (i.e., during the E wave). If this hypothesis is valid, then it should be possible to establish a range of values for the optimal formation time in normal healthy hearts based on the normal LV ejection fraction (*EF*), an existing standard measure for LV function. The desired range can be obtained from the following equation (see *Methods*):

$$T = \frac{4(1-\beta)}{\pi}\cdot\alpha^3\cdot EF. \qquad [1]$$

The variable α is a LV geometry parameter defined as

$$\alpha \equiv \frac{EDV^{1/3}}{\bar{D}}, \qquad [2]$$

where EDV is the LV end-diastolic volume and $\bar{D}$ is the time-averaged mitral valve diameter. The parameter β is the fraction of the stroke volume contributed from LV A wave filling (i.e., atrial contraction) and is equal to 0.2 in a normal heart at rest. Therefore, the LV vortex formation time under normal conditions can be calculated as $T \approx \alpha^3 \cdot EF$. From this relationship, one can observe variations of the vortex formation time for different values of the ejection fraction and ventricular geometry parameter (α). For example, the solid curved line in Fig. 2 indicates that, for $EF = 0.65$ (i.e., the normal range), the vortex formation time increases with α. Calculating α based on normal human LV values for the end-diastolic volume (EDV) and the average mitral valve diameter ($\bar{D}$), α ranges between 1.7 and 2.0 (22). Therefore, during normal LV function, the E wave phase is completed within a vortex formation time $3.3 < T < 5.5$. This

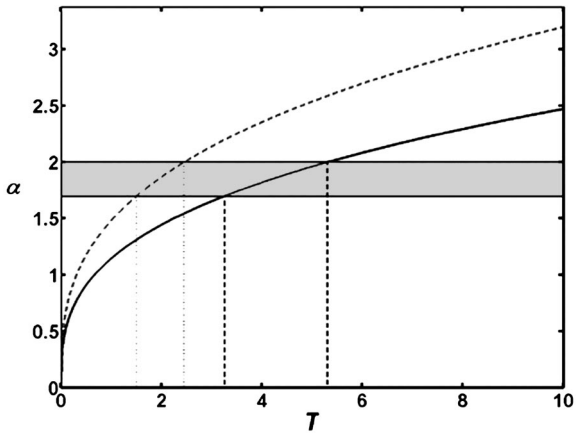

Fig. 2. Quantitative relationship between LV geometry parameter (α), LV ejection fraction, and approximate vortex formation time (T). Horizontal gray band indicates normal range of LV geometry parameter (α). Solid curved line, LV ejection fraction = 0.65 (i.e., normal LV function); dashed curved line, LV ejection fraction = 0.3 (e.g., DCM). The vortex formation time (T) corresponding to normal LV function (i.e., values bounded by vertical dashed lines) is consistent with the range of optimal vortex formation found in previous *in vitro* experiments (14, 21). The vortex formation time corresponding to a reduced LV ejection fraction (i.e., values bounded by vertical dotted lines) is lower than the optimal range.

range is consistent with the optimal range of vortex formation time found in previous *in vitro* vortex formation studies (14, 21) and, interestingly, also has been identified as the optimal range of vortex formation for aquatic locomotion (21, 23). This observed robustness of the optimal vortex formation index suggests that pathologies in biological fluid transport will be manifested in changes to this governing parameter.

Indeed, remodeling pathologies of the LV such as mitral valve stenosis are reflected in an increase of the LV geometry parameter α (via a decrease in $\bar{D}$), leading to a concomitant increase in the vortex formation time of up to an order of magnitude (17). When the LV ejection fraction is reduced, e.g., $EF \rightarrow 0.3$ in the case of dilated cardiomyopathy (DCM; ref. 22), the vortex formation time drops significantly from the optimal value to the range 1.5 to 2.5 (Fig. 2, dashed curved line). Hence, cardiac pathologies affecting the LV geometry (α) and/or its function (EF) appear in deviations of the vortex formation time from its optimal range $T^* \approx 4$.

In further support of these results, two independent studies were conducted in the Division of Cardiology at the University of California at San Diego and in the Division of Engineering and Applied Science at the California Institute of Technology. A total of 110 volunteers from 5 to 84 years of age were randomly selected to undergo transthoracic echocardiography for imaging the left ventricle from the apical view.

Fig. 3 depicts the distribution of total vortex formation time (i.e., at the end of the E wave) versus age for the adults (>20 years old) measured in the studies ($n = 80$). Blue circles indicate the calculated values of vortex formation time for blind test cases where no prior information about patients' cardiac health was obtained, and red squares indicate the data for patients with DCM. The distribution of vortex formation time corresponding to the blind test converges to values in the anticipated optimal range between 3.5 and 5.5. The standard deviation from a least-squares linear fit to the data (SD = 1.03; see Fig. 3), and the corresponding histogram (Fig. 3 *Inset*) provide quantitative bounds for the range of vortex formation times for the blind test population. The distribution of vortex formation times corresponding to the DCM patients is located below the optimal range, as predicted by the aforementioned relationship between vortex formation time and ejection fraction (Fig. 2). The

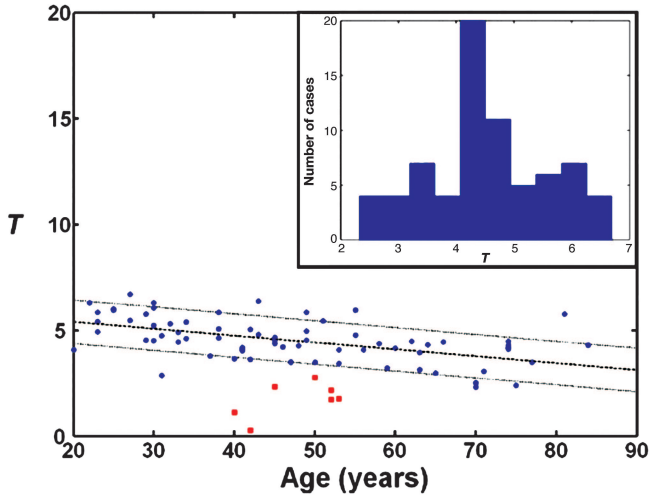

Fig. 3. Vortex formation time in adult humans from blind test and those with DCM. Blue circles, blind test; red squares, DCM. Least-squares linear fit to blind test data are indicated by dashed black line. Dotted black lines indicate one standard deviation from the linear fit (SD = 1.03). (*Inset*) Histogram of vortex formation time data from blind test and DCM populations.

hypothesis of a distinction between the vortex formation time distributions corresponding to the blind test population LV function and the population with DCM is confirmed at a 95% confidence level by P value calculations from Mann–Whitney and Student's t tests of the data sets ($P = 2.1 \times 10^{-5}$ and 1.2×10^{-4}, respectively).

A likely source of scatter in the data arises from the use of the approximated vortex formation time definition of T^*, which incorporates the maximum mitral valve exit diameter rather than the time-dependent diameter (see *Methods*). This approximation was necessary given the limited temporal and spatial resolution of the available measurement techniques. Future studies will benefit from advances in nonintrusive measurement resolution, which should result in a better understanding of how specific pathophysiological events are manifested in the relationship between transmitral jet diameter and the vortex formation time, $D(T^*)$, as introduced in ref. 17. It is important to note that the blind test population in Fig. 3 may contain cases of disease progression toward other cardiac pathologies besides DCM. Although these cases could not be specifically delineated in this study, they are also expected to deviate from the optimal range of vortex formation time. The sharply peaked nature of the histogram in Fig. 3 indicates that the index of optimal vortex formation introduced here is a sensitive measure of cardiac health.

Methods

Human Subject Measurement Protocol. To evaluate the LV diastolic filling event and its relationship with cardiac function, the set of parameters required to determine the dimensionless vortex formation time T^* were recorded. The mitral annulus diameter was used as the exit diameter ($\bar{D}$), and was measured from long-axis apical views of the LV at the peak of diastole (i.e., the largest measurable diameter) and from M mode Doppler images. Mean blood flow velocity from the atrium to the ventricle of the left heart (i.e., transmitral flow $\bar{U}$) was obtained from pulsed-wave Doppler measurements in the immediate downstream vicinity of the opened mitral valve leaflets. Vortex formation time was then calculated for each case based on the approximate definition

$$T = \frac{\bar{U}\cdot t}{\bar{D}}, \qquad [3]$$

where t is the duration of the E wave.

Data from human subjects have been obtained through a protocol and Institutional Review Board approved by the University of California at San Diego medical school and with the written consent of the volunteers. Ultrasound data from human subjects were evaluated in double-blind studies by two independent observers. A total of six measurements were recorded for each parameter (i.e., $\bar{U}$, $\bar{D}$, and t). A corresponding random error of $\pm$ 5% is associated with each presented data point.

Derivation of Ejection Fraction and Vortex Formation Time. The term ejection fraction refers to the ratio of LV stroke volume to the LV volume at the end of diastole:

$$EF = \frac{EDV - ESV}{EDV} = \frac{SV}{EDV}, \qquad [4]$$

where EDV is the LV volume at the end of diastole (LV filling), ESV is the LV volume at the end of systole (LV ejection), and SV is the stroke volume. The stroke volume can be rewritten as

$$SV = V_E + V_A = \bar{U}_E\cdot t_E\cdot \frac{\pi}{4}\bar{D}^2 + \bar{U}_A\cdot t_A\cdot \frac{\pi}{4}\bar{D}^2, \qquad [5]$$

where V_E and V_A are contributions of the E and A waves during LV filling and $\bar{D}$ is the time-averaged mitral valve diameter. Multiplying both sides of Eq. **5** by $4/\pi\bar{D}^3$ and replacing the stroke volume with Eq. **4**:

$$\frac{4}{\pi\cdot\bar{D}^3}\cdot(EF\cdot EDV) = \frac{\bar{U}_E\cdot t_E}{\bar{D}} + \left(\frac{4}{\pi\bar{D}^3}\cdot V_A\right), \qquad [6]$$

or

$$T^* \approx \frac{4}{\pi\cdot\bar{D}^3}\cdot[(EF\cdot EDV) - V_A], \qquad [7]$$

where the approximation sign arises implicitly from the assumption that $T^* \approx \bar{U}t/\bar{D} = T$. Denoting β, the fraction of the stroke volume contributed from LV A wave filling (i.e., atrial contraction) and defining a LV geometry parameter

$$\alpha \equiv \frac{EDV^{1/3}}{\bar{D}}, \qquad [8]$$

the relationship between LV vortex formation time and the LV ejection fraction is established:

$$T = \frac{4(1-\beta)}{\pi}\cdot\alpha^3\cdot EF. \qquad [9]$$

We thank the Vascular Imaging Research Center, Department of Radiology, Veterans Affairs Medical Center/University of California, San Francisco, for providing *in vivo* magnetic resonance images. This work was supported by the National Science Foundation.

1. Echeverria, H. H., Bilsker, M. S., Myerburg, R. J. & Kessler, K. M. (1983) *Am. J. Med.* **75,** 750–755.
2. Ohno, M., Cheng, C. P. & Little, W. C. (1994) *Circulation* **89,** 2241–2250.
3. Vasan, R. S., Larson, M. G., Benjamin, E. J., Evans, J. C., Reiss, C. K. & Levy, D. (1999) *J. Am. Coll. Cardiol.* **33,** 1948–1955.
4. Kilner, P. J., Yang, G. Z., Wilkes, A. J., Mohiaddin, R. H., Firmin, D. N. & Yacoub, M. H. (2000) *Nature* **404,** 759–761.
5. Yellin, E. L. & Meisner, J. S. (2000) *Cardiol. Clin.* **18,** 411–433.
6. Zile, M. R. & Brutsaert, D. L. (2002) *Circulation* **105,** 1387–1393.
7. Hasegawa, H., Little, W. C., Ohno, M., Brucks, S., Morimoto, A., Cheng, H. J. & Cheng, C. P. (2003) *J. Am. Coll. Cardiol.* **41,** 1590–1597.
8. Pedrizzetti, G. & Domenichini, F. (2005) *Phys. Rev. Lett.* **95,** 108101.
9. Bellhouse, B. J. (1972) *Cardiovasc. Res.* **6,** 199–210.
10. Reul, H., Talukder, N. & Muller, W. (1981) *J. Biomech.* **14,** 361–372.

11. Kim, W. Y., Walker, P. G., Pedersen, E. M., Poulsen, P. K., Oyre, S., Houlind, K. & Yoganathan, A. P. (1995) *J. Am. Coll. Cardiol.* **26,** 224–238.
12. Maxworthy, T. (1977) *J. Fluid Mech.* **81,** 465–495.
13. Didden, N. (1979) *Z. Angew. Math. Phys.* **30,** 101–116.
14. Gharib, M., Rambod, E. & Shariff, K. (1998) *J. Fluid Mech.* **360,** 121–140.
15. Dabiri, J. O. & Gharib, M. (2004) *J. Fluid Mech.* **511,** 311–331.
16. Krueger, P. S. & Gharib, M. (2003) *Phys. Fluids* **15,** 1271–1281.
17. Dabiri, J. O. & Gharib, M. (2005) *Proc. R. Soc. London Ser. B* **272,** 1557–1560.
18. Grodecki, P. V. & Klein, A. L. (1993) *Echocardiography* **10,** 213–234.
19. Mohseni, K. & Gharib, M. (1998) *Phys. Fluids* **10,** 2436–2438.
20. Dabiri, J. O. & Gharib, M. (2004) *Phys. Fluids* **16,** L28–L30.
21. Dabiri, J. O. & Gharib, M. (2005) *J. Fluid Mech.* **538,** 111–136.
22. Fuster, V., Alexander, R. W., O'Rourke, R. A., Roberts, R., King, S. B., Prystowsky, E. N. & Nash, I. (2004) *Hurst's The Heart* (McGraw-Hill, New York).
23. Linden, P. F. & Turner, J. S. (2004) *Proc. R. Soc. London Ser. B* **271,** 647–653.